Alzheimer's & Dementia

Featured Article

Zfra restores memory deficits in Alzheimer's disease triple-transgenic mice by blocking aggregation of TRAPPC6AΔ, SH3GLB2, tau, and amyloid β, and inflammatory NF-κB activation

Ming-Hui Lee[a,1], Yao-Hsiang Shih[b,1], Sing-Ru Lin[a,1], Jean-Yun Chang[a,1], Yu-Hao Lin[a], Chun-I Sze[b,*], Yu-Min Kuo[b,*], Nan-Shan Chang[a,c,d,e,f,*]

[a]Institute of Molecular Medicine, College of Medicine, National Cheng Kung University, Tainan, Taiwan, ROC
[b]Department of Cell Biology and Anatomy, College of Medicine, National Cheng Kung University, Tainan, Taiwan, ROC
[c]Advanced Optoelectronic Technology Center, National Cheng Kung University, Tainan, Taiwan, ROC
[d]Center of Infectious Disease and Signaling Research, College of Medicine, National Cheng Kung University, Tainan, Taiwan, ROC
[e]Graduate Institute of Biomedical Sciences, College of Medicine, China Medical University, Taichung, Taiwan, ROC
[f]Department of Neurochemistry, New York State Institute for Basic Research in Developmental Disabilities, New York, NY, USA

Introduction: Zinc finger-like protein that regulates apoptosis (Zfra) is a naturally occurring 31-amino-acid protein. Synthetic peptides Zfra1–31 and Zfra4–10 are known to effectively block the growth of many types of cancer cells.
Methods: Ten-month-old triple-transgenic (3×Tg) mice for Alzheimer's disease (AD) received synthetic Zfra peptides via tail vein injections, followed by examining restoration of memory deficits.
Results: Zfra significantly downregulated TRAPPC6AΔ, SH3GLB2, tau, and amyloid β (β) aggregates in the brains of 3×Tg mice and effectively restored their memory capabilities. Zfra inhibited melanoma-induced neuronal death in the hippocampus and plaque formation in the cortex. Mechanistically, Zfra blocked the aggregation of amyloid β 42 and many serine-containing peptides in vitro, suppressed tumor necrosis factor–mediated NF-κB activation, and bound cytosolic proteins for accelerating their degradation in ubiquitin/proteasome-independent manner.
Discussion: Zfra peptides exhibit a strong efficacy in blocking tau aggregation and amyloid β formation and restore memory deficits in 3×Tg mice, suggesting its potential for treatment of AD.
© 2017 The Authors. Published by Elsevier Inc. on behalf of the Alzheimer's Association. This is an open access article under the CC BY-NC-ND license (http://creativecommons.org/licenses/by-nc-nd/4.0/).

Keywords: Zfra; TRAPPC6A; SH3GLB2; WWOX; Peptide polymerization; Protein degradation; Neurodegeneration

1. Introduction

Zinc finger-like protein that regulates apoptosis (Zfra) is a 31-amino-acid protein, possessing two cysteines and one histidine in the amino acid sequence [1–4]. Zfra is one of the binding proteins for tumor suppressor WW domain-containing oxidoreductase (WWOX, FOR, or WOX1) [5–9]. Substantial evidence shows that WWOX is involved in neural diseases. WWOX controls the functional activities of glycogen synthase kinase 3 beta (GSK-3β) and other enzymes in hyperphosphorylating tau and thereby prevents neurodegeneration [9–11]. Downregulation of WWOX protein is associated with neurodegeneration such as Alzheimer's disease (AD) [9–12]. Alteration of *WWOX/Wwox* gene, for example, null mutations and missense mutations, results in severe neural diseases and metabolic disorders, including ataxia, epilepsy, dementia, neurodegeneration, growth retardation,

---

abnormal HDL (high density lipoprotein) lipid metabolism, and early death [9,13–16]. Under WWOX deficiency or dysfunction, a cascade of protein aggregation, including TRAPPC6AΔ (trafficking protein particle complex 6A delta, TPC6AΔ), TIAF1 (TGFβ1-induced anti-apoptotic factor 1), tau, and amyloid β (Aβ), occurs in the mitochondria and leads to apoptosis [17–20]. Both TPC6AΔ and TIAF1 tend to aggregate in the brain extracellular matrix when WWOX is deficient or dysfunctional. However, transiently overexpressed WWOX induces mitochondrial apoptosis in vitro [21,22]. Transgenic mutant WWOX proteins cause mitochondrial dysfunction by affecting the respiratory complex in *Drosophila* [23].

Zfra counteracts the function of WWOX by blocking Tyr33 phosphorylation [2–4]. Transiently overexpressed WWOX induces mitochondrial apoptosis through cytochrome c release [21,22], whereas Zfra binds and blocks WWOX-mediated apoptosis without causing cytochrome c release [3,4]. Recently, we demonstrated that when nude mice and BALB/c mice receive a synthetic full-length Zfra1–31 or a truncated Zfra4–10 peptide via tail veins, these mice resist the growth, metastasis, and stemness of melanoma xenografts and 11 other malignant cancer cells [24]. The injected Zfra peptide mainly goes to the spleen but not other organs and activates a novel non-T/non-B lymphocyte, designated Hyal-2$^+$ CD3$^-$ CD19$^-$ Z cell, to block cancer growth and metastasis [24,25]. Z cell possesses a memory function in blocking cancer growth.

Here, we determined that Zfra restores memory deficits in triple-transgenic mice for AD. Zfra works by accelerating protein degradation and blocking TRAPPC6AΔ, tau, and Aβ aggregation. Under WWOX deficiency or dysfunction or sustaining stimulation of cells with transforming growth factor beta (TGF-β), a cascade of protein aggregation occurs [17–20]. TRAPPC6AΔ starts to undergo Ser35 phosphorylation, then polymerizes, and initiates TIAF1 aggregation with Ser37 phosphorylation. The TRAPPC6AΔ/TIAF1 complex induces caspase 3 activation, dephosphorylation of membrane amyloid precursor protein (APP) at Thr688 and degradation for Aβ formation, and pT181-tau aggregation [17–20]. Notably, Zfra suppressed WWOX phosphorylation at Ser14. pSer14-WWOX appears to be associated with disease progression and severity.

2. Methods

2.1. Peptides

Zfra and serine-containing peptides were synthesized by Genemed Synthesis (San Antonio, TX, USA): (1) Zfra1–31, MSSRRSSSCKYCEQDFRAHTQKNAATPFLAN; (2) Zfra4–10, RRSSSCK; (3) WWOX7-21, AGLDDTDSEDELPPG; (4) pS14-WWOX7-21, AGLDDTD**pS**EDELPPG; (5) WWOX286-299, DYWAMLAYNRSKLC; (6) pY287-WWOX286-299, D**pY**WAMLAYNRSKLC; (7) TPC6A24-38, DPGPGGQKMSLSVLE; (8) pS35-TPC6A24-38, DPGPG GQKMSL**pS**VLE; (9) TPC6A84-100, KDLWVAVFQKQ MDSLR; (10) ANKRD40266-281, RIQNPSLRENDFIEIE; (11) pS271-ANKRD40266-281, RIQNP**pS**LRENDFIEIE; (12) tetramethylrhodamine-labeled Zfra (TMR-Zfra), the full-length Zfra1–31 was labeled with a red-fluorescent Texas Red maleimide fluorescent probe tetramethylrhodamine. The peptide stocks were made as 10 mM in degassed sterile Milli-Q water. Each tube was flushed with nitrogen and stored in −80°C freezer. For tail vein injections, peptides were freshly prepared in degassed Milli-Q water at 1–4 mM in 100-μL Milli-Q. GenBank accession for ANKRD40 is EU164539. Aβ peptides were from AnaSpec: (1) Aβ42: DAEFRHDSGYEVHHQKLVFFAEDVGSNKG AIIGLMVGGVVIA; (2) Aβ40: DAEFRHDSGYEVHH QKLVFFAEDVGSNKGAIIGLMVGGVV. Where indicated, Zfra peptide was mixed and incubated with an aforementioned peptide for 12–24 hours at room temperature, followed by determining peptide aggregation using sodium dodecyl sulfate polyacrylamide gel electrophoresis (SDS-PAGE) and silver staining.

2.2. Antibodies

Homemade antibodies used in the experiments were against Zfra, pS8-Zfra, and WWOX (WOX1) [10,17,18,20,21]. Commercial antibodies used were as follows: (1) monoclonal Aβ antibody (AbD/Serotec), (2) monoclonal paired helical filament (PHF)–tau antibody (Pierce/Invitrogen), (3) EGFP (Santa Cruz Laboratory), (4) His tag antibody (Sigma), (5) pT181-tau antibody (Biosource) [17,21]. An approved protocol for rabbit use in antibody production was from the IACUC of the National Cheng Kung University Medical College. Antibodies were produced using the following synthetic peptides: (1) WWOX7-21, CAGLDDTDSEDELPPG; (2) pS14-WWOX7-21, CAGLDDTD**pS**EDELPPG; (3) TPC6A, CKDLWVAVFQKQMDSLR, amino acid #84-100 for pan-specific antibody production. These peptides were conjugated with keyhole limpet hemocyanin (KLH) via the *N*-terminal cysteine for antibody production in rabbits (using an Antibody Production and Purification kit from Pierce) [21,26,27]. The *N*-terminal cysteine in each peptide sequence was added for covalently conjugating with KLH. The specific pS14-WWOX antibody was purified as described [27]. The specificity of the antisera was tested using the synthetic peptides to block immunoblots. Where indicated, Western blotting was carried out as described [1,8,10,14]. In addition, we generated antibody against self-polymerizing SH3GLB2 (SH3 domain-containing GRB2-like endophilin B2), using the synthetic peptide NH-CDACKARLKKAKAAEAK-COOH (amino acid 170–185).

2.3. Animals

All experiments were carried out in accordance with the National Institutes of Health Guidelines for animal research

(Guide for the Care and Use of Laboratory Animal) and approved by the National Cheng Kung University Institutional Animal Care and Use Committee. The 3×Tg mice (B6; 129-Psen1tm1Mpm Tg[APPSwe, tauP301L]1Lfa/ Mmjax) [28], were obtained from the Jackson Laboratory (Bar Harbor, ME, USA) and housed in a controlled room (temperature 23 ± 1°C, humidity 55± 5%, 12-hour light/ 12-hour dark cycle, light cycle begins at 06:00) located in the Laboratory Animal Center of National Cheng Kung University (Tainan, Taiwan) with unrestricted access to food and water. All mice were genotyped using a protocol provided by the Jackson Laboratory. The 3×Tg mice develop intracellular Aβ immuno-positive staining as early as 3–4 months and aggregates of hyperphosphorylated tau in the hippocampus around 12 months of age. Impaired synaptic transmission and long-term potentiation are evident about 6 months of age. At the age of 10 months (body weight: 31∼35 g), five 3×Tg mice received four consecutive weekly injections of Zfra4–10 solution (2 mM in phosphate buffered saline [PBS], 100 μL each injection) from the tail veins. Another five mice underwent the same procedure with PBS injections served as a sham control group. After necessary behavioral tests shown in the following, mice were sacrificed by CO_2 anesthesia (75% CO_2/25% O_2) and perfused with 10-mL PBS (to reduce background in tissue section staining with specific antibodies). Brains were then rapidly harvested.

2.4. Novel object recognition test

The experiment was performed from 6 PM each day [29–32]. One week after the last injection of Zfra4–10 solution, mouse was habituated to a polycarbonate box (47.5 cm × 25.8 cm × 21 cm) for 10 minutes per day for 3 consecutive days. On the next day, each mouse was placed back into the same box containing two identical objects (glass bottle, 4-cm diameter and 6.5-cm high) separately positioned 7 cm away from a wall. The cumulative times spent by the mouse in exploring each of the objects were recorded during a 5-minute period. Two hours later, the mouse was reintroduced into the box for the short-term memory (STM) test. One of the two objects was replaced by a new one (white Lego bricks, 3 cm × 3 cm × 6 cm). For the long-term memory (LTM) test, the mouse was reintroduced into the box after 24 hours. One of the two objects was replaced by a new one (white plastic bottle, 3.5 cm diameter and 7.2 cm high). The times spent in exploring each object during a 5-minute period were recorded in either the STM or the LTM test. All of the objects were cleaned by 70% alcohol between trials to reduce olfactory cues.

2.5. Morris water maze test

The hippocampus-dependent spatial learning and memory was evaluated by Morris water maze test, 1 day after the completion of novel object recognition test [29–32].

The Morris water maze was performed in a custom-made circular pool with a diameter of 120 cm and a wall height of 31 cm, which was filled with clear tap water at a temperature of 24 ± 1°C and depth of 25 cm. The circular escape platform made of transparent Plexiglas (diameter 10 cm) was submerged 1 cm below the surface of the water. During all trials of spatial navigation, the location of the hidden platform was kept constant. Animals were given a one-session training, began at 18:00, per day for 4 days. Each session consisted of four swim trials (maximum 120 seconds per trial) with different quadrant starting positions for each trial. On the fifth day morning, animals were subjected to probe test. During the probe test, mouse was placed in the pool in the southwest position, the longest distance from the previous platform position (northeast), and the mouse was allowed to swim for 60 seconds without platform present. The whole process was recorded by a CCD camera, and the escape latency (i.e., time to reach the platform, in seconds), path length, and swim speed (cm/s) were analyzed by EthoVision video tracking system (Noldus Information Technology, Wageningen, Netherlands).

2.6. Brain processing and immunohistochemistry

After removing the brains, the right hemispheres were stored at −70°C, whereas the left hemispheres were fixed in 4% buffered paraformaldehyde at 4°C ready for frozen sections. Coronal sections (30-μm thickness) of the right hemisphere were collected in cryoprotectant solution (30% ethylene glycol, 20% glycerol, 50-mM sodium phosphate buffer, pH 7.4) and stored at −20°C. The brain sections were washed, blocked with goat serum (3% in PBS/0.5% Triton X-100) for 1 hour, and probed with the following primary antibodies: pS412-tau (1:1000, AS-55418P, Anaspec, Fremont, CA, USA) and a mixture of 6E10 (1:1000, against Aβ 1-17, Signet, Dedham, MA, USA) and 4G8 (1:1000, against Aβ 17-24, Signet). The floating sections were incubated in primary antibodies for 16 hours at 4°C, then incubated with appropriate secondary antibodies (1:1000, Vector Laboratories, Burlingame, CA, USA) and an avidin-biotin peroxidase (Vector) using 3, 3′-diaminobenzidine as the substrate. A parallel section stained without primary antibody served as negative control.

For the Aβ-positive cell counting, two sections, representing dorsal hippocampus (stereotaxic reference: bregma −2.2 ± 0.2 mm) and ventral hippocampus (stereotaxic reference: bregma −3.3 ± 0.2 mm), were selected. Only those cells with Aβ immunostaining signal intensity higher than a given background threshold, determined by the ImagePro plus 6.0 software (Bethesda, MD, USA), and with clear and identifiable cell bodies were counted. The background intensity threshold was fixed and applied to all sections.

To analyze pS412-tau signals, photomicrographs were taken from dorsal and ventral hippocampus using an Axio-camMRc digital camera connected to a computer equipped

with Axiovision 4.8 software (Carl Zeiss, Oberkochen, Germany). The intensity of pS412-Tau immunoreactivity was evaluated by means of a relative optical density (ROD), which was obtained after transforming the RGB format to gray-scale format. ROD of the background was determined in unlabeled portions using ImagePro plus 6.0 software (Bethesda, MD, USA), and the value was subtracted for correction. The background intensity threshold was fixed and applied to all sections.

2.7. Thioflavin-S staining

The mounted slice was incubated with 0.2% (w/v) thioflavin-S in PBS for 30 minutes to stain for matured (β-pleated sheet-containing) amyloid plaques. After washing the tissue three times with PBS, the slice was dehydrated in sequence with 50%, 75%, 95%, and 100% ethanol. After dehydration, the slice was submerged in Xylene for 10 minutes and attached to glass slide with mounting gel.

2.8. Statistical analysis

All experimental results were represented as mean ± standard error of the mean. The results for novel object recognition test, probe test of Morris water maze, relative ventricle area, and relative optical density of pS412-tau immunoreactivity were analyzed by two-tailed Mann–Whitney test, whereas the Aβ-positive cell number was analyzed by two-tailed unpaired t-test. The Morris water maze learning section results were analyzed using a repeated mixed-model analysis of variance with training session as within-subject factor and the Zfra injection as between-subject factor. Bonferroni post hoc tests were performed if significant ($P < .05$) main effects were found.

2.9. Neurodegeneration model in tumor-growing mice

Six- to eight-week-old male nude (BALB/cAnN.Cg-*Foxn1*[nu]/CrlNarl) mice (National Laboratory Animal Center, Taiwan) were used. Mice were intravenously injected into tail veins with 100 μL of Zfra1–31 or Zfra4–10 (2 mM), or sterile Milli-Q water. After injection for 1–8 weeks, mouse melanoma B16F10 or human glioma 13-06-MG cells (2–2.5×10^6 cells/100-μL saline) were then inoculated in subcutaneous sites at both flanks. Tumor volumes were measured daily and calculated using the equation: $D \times (d)^2/2$, where D and d are the major and minor diameters, respectively. At indicated time point, mouse organs, including brain, lung, spleen, and liver, were harvested and fixed with 4% paraformaldehyde. IHC was carried out using indicated specific antibodies to determine protein expression in tissues and organs. Where indicated, TMR-Zfra was used to stain spleen, brain, and lung tissues. Z-cell distribution in organs was determined under fluorescence microscopy.

2.10. Human hippocampal tissues, tissue extractions for filter retardation assay, and tissue sections for immunohistochemistry

We obtained human postmortem frozen hippocampal tissues and fixed-tissue sections from hippocampi from the Brain Bank of the Department of Pathology, University of Colorado Health Sciences Center (by Dr. CI Sze, before 2005) [10,17,33]. Institutional review board approval was waived. Informed consents were obtained from the family members of the deceased patients. Where indicated, the tissue samples were homogenized in a lysis buffer and the insoluble fractions subjected to filter retardation assay [17]. Presence of Zfra, pS8Zfra, and Aβ was determined by using specific antibodies in dot blotting and quantified [1,3,17].

2.11. Promoter activation assay

We examined whether Zfra affected tumor necrosis factor (TNF)-mediated activation of promoter governed by NF-κB [10,20,33]. COS7 cells were transfected with a promoter construct for NF-κB using green fluorescent protein (GFP) as a reporter by electroporation, followed by exposure to TNF (50 ng/mL) for 24 hours. Both positive and negative controls were also tested in each experiment.

3. Results

3.1. Zfra rescues the age-related decline of hippocampus-dependent memory in 3×Tg-AD mice

A triple-transgenic mouse (3×Tg) model of AD, expressing mutant Psen1(M146V), APPSwe, and tau (P301L), was used [28]. Zfra4–10 peptide was synthesized (>95% pure) and freshly prepared before use [24]. One week after four injections with Zfra4–10 via tail veins, 11-month-old 3×Tg mice were subjected to novel object recognition test for hippocampus-dependent, nonspatial learning and memory [29–32]. During the 5-minute acquisition phase, both the sham and Zfra mice spent approximately equal exploring times on each object (Fig. 1A, Mann–Whitney $U = 10$, $P > .5$), indicating no position preferences in the task environment. In the short-term memory task (2 hours after the acquisition phase), the Zfra group showed a marginal, but not significant, increase in the exploring times of the novel object (Fig. 1A, Mann–Whitney $U = 3$, $P = .074$), whereas in the long-term memory task (24 hours after the acquisition phase), the novel object exploring times of the Zfra group were significantly higher than those of the sham group (Fig. 1A, Mann–Whitney $U = 2$, $P = .008$). These results suggest that the hippocampus-dependent, nonspatial long-term memory of 3×Tg mice was increased by Zfra treatment. That is, higher exploring times with the novel object means better memory performance.

One day after the novel object recognition test, the Zfra- and sham-treated 3×Tg mice were subjected to Morris
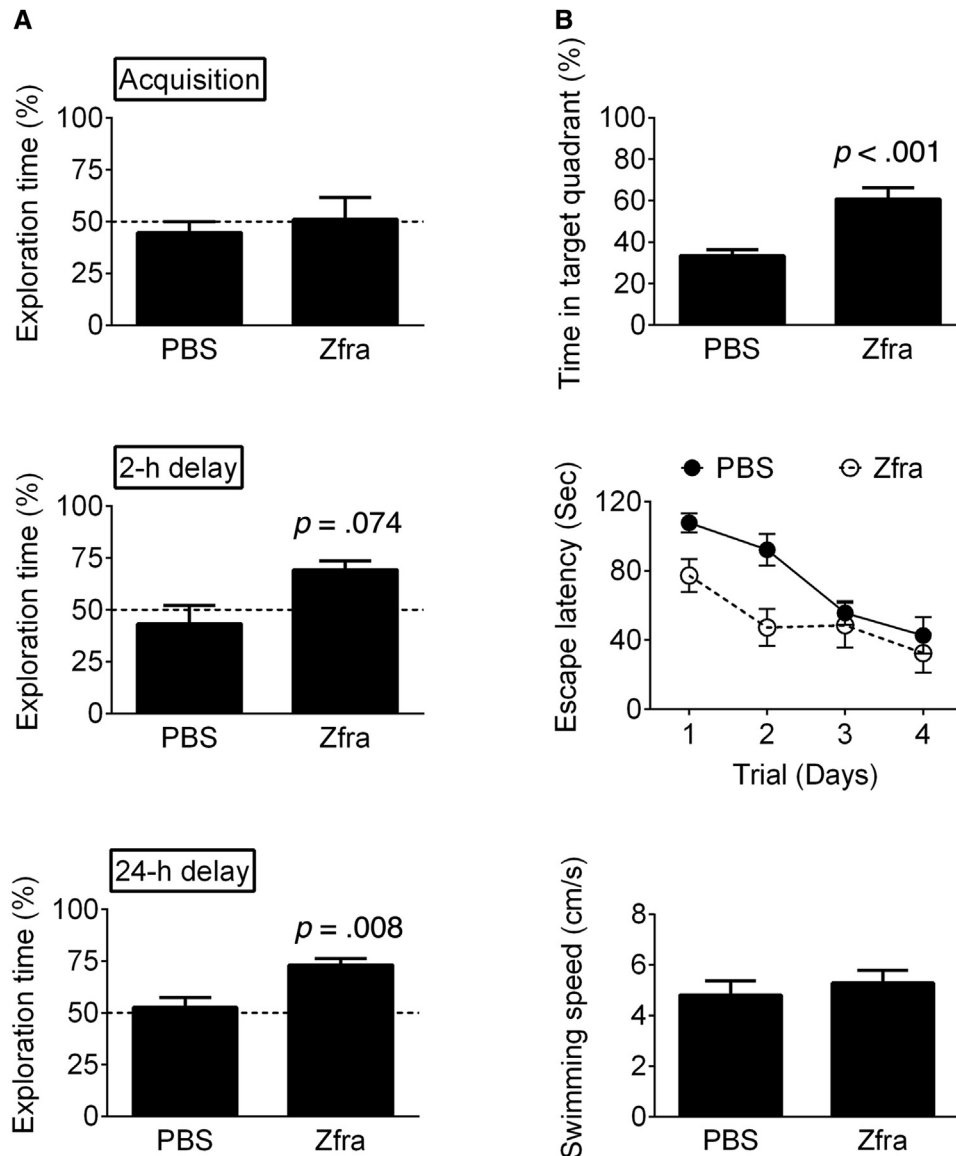
Fig. 1. Effect of Zfra peptide on learning and memory of 3×Tg mice. (A) The nonspatial learning and memory were determined by novel object recognition task. The abilities of nonspatial memory are expressed as the percentages of novel object exploring time (time spent on novel object/time spent on both objects) during acquisition, short-term (2 hours) delay, and long-term (24 hours) delay (PBS group, $n = 6$; Zfra group, $n = 5$). (B) The spatial learning and memory were determined by Morris Water Maze: latency of training sessions; probe test in water maze; swimming speeds. Statistics: Zfra versus respective PBS group, two-tailed Mann–Whitney test (PBS group, $n = 12$; Zfra group, $n = 10$). Abbreviations: PBS, phosphate buffered saline; Zfra, zinc finger-like protein that regulates apoptosis.

water maze to evaluate the hippocampus-dependent, spatial learning and memory. Both the sham and Zfra groups showed a time-dependent decrease of escape latency (Fig. 1B; $F = 4.9$, df 3/32, $P = .006$). Furthermore, the escape latencies were comparable between these two groups (Fig. 1B; $F = 0.2$, df 1/32, $P > .5$), indicating that the learning capabilities were not affected by Zfra treatment. In the probe test with the platform removed, the Zfra mice spent more time in the targeted quadrant than that of sham mice (Fig. 1B; Mann–Whitney $U = 2$, $P < .001$). The swim velocities in these two groups were similar (Fig. 1B; Mann–Whitney $U = 11$, $P > .5$).

3.2. Zfra reduces the AD-related pathologies in 3×Tg mice

Zfra treatment significantly reduced the numbers of Aβ-positive cells in the dorsal and ventral hippocampi of the 3×Tg mice (Fig. 2A and B). As stained with thioflavin-S, the presence of cortical Aβ plaques was found in the 10-month-old 3×Tg mice, and Zfra significantly suppressed the plaque formation (Fig. 2C). Furthermore, the relative levels of pS412-tau were also increased in the dorsal and ventral hippocampi of the 3×Tg mice (Fig. 3). Detail analysis of the expression patterns of pS412-tau revealed that
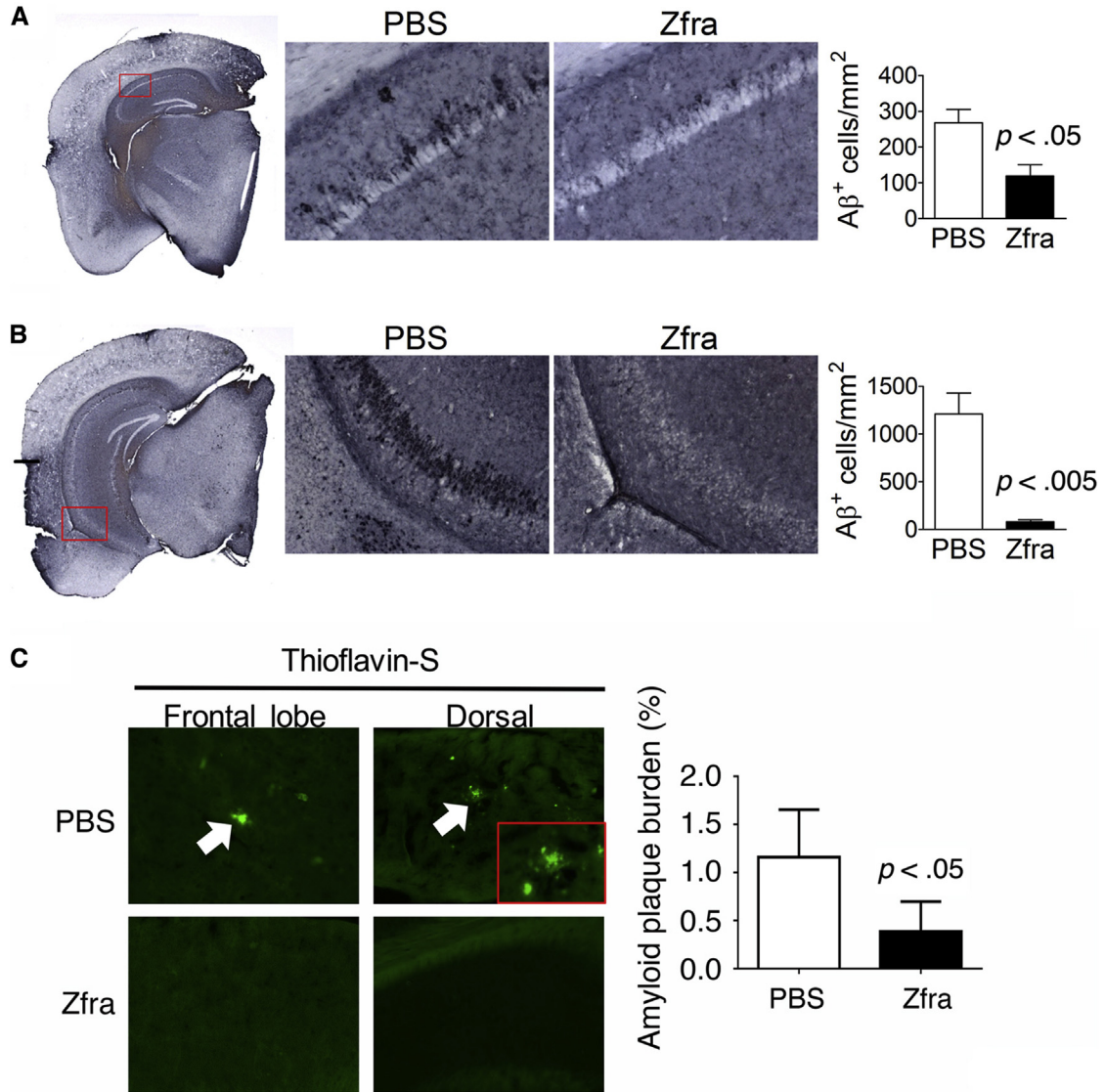
Fig. 2. Effect of Zfra peptide on Aβ deposition in 3×Tg mice. Representative micrographs of Aβ-positive cells are shown on the left panels, the boxed regions are enlarged and shown on the middle, and the quantitative results are shown on the right. (A) Dorsal hippocampus. (B) Ventral hippocampus. *$P < .05$ versus respective PBS group, two-tailed unpaired t-test (PBS group, $n = 3$; Zfra group, $n = 5$). Also, representative micrographs of cortical Aβ plaques (white arrows) are shown for the PBS controls and Zfra-treated mice on the left panel (C), and the data quantified on the right. Statistics: Zfra versus respective PBS group, two-tailed unpaired t-test (PBS group, $n = 3$; Zfra group, $n = 5$). Abbreviations: Aβ, amyloid β; Zfra, zinc finger-like protein that regulates apoptosis.

the elevated pS412-tau signals mainly localized in the stratum oriens and stratum radiatum of the hippocampus, and Zfra significantly reduced the expression in both regions (Fig. 3A and B). These results are in agreement with the findings of AD pathology that neurofibrillary tau burden in the hippocampus are frequently restricted to the stratum radiatum and stratum lacunosum [34,35]. By using specific pT181-tau antibody for PHF-tau [17], tau aggregates are shown in the cortex and Zfra significantly blocked the aggregation (Fig. 3C). Recently, we demonstrated that TPC6AΔ, an intra-*N*-terminal deletion of TPC6A, forms cortical plaques starting from mid-ages of normal humans [17]. Zfra significantly suppressed the expression of intra-

cellular pS35-TPC6AΔ and blocked the formation of extracellular pS35-TPC6AΔ plaques (Fig. 3D). SH3GLB2 undergoes self-polymerization via BAR domain [36]. Zfra effectively blocked the aggregation of SH3GLB2 by ∼70% (Fig. 3E).

3.3. Zfra does not induce neurogenesis in 3×Tg mice

We examined whether Zfra-mediated restoration of memory and behavioral deficits in the 3×Tg mice is involved in neurogenesis [29–32]. Zfra treatment did not change the number of BrdU⁺ cells ($t = 0.4$, $P > .5$) in the subgranular zone of hippocampus in the 3×Tg mice
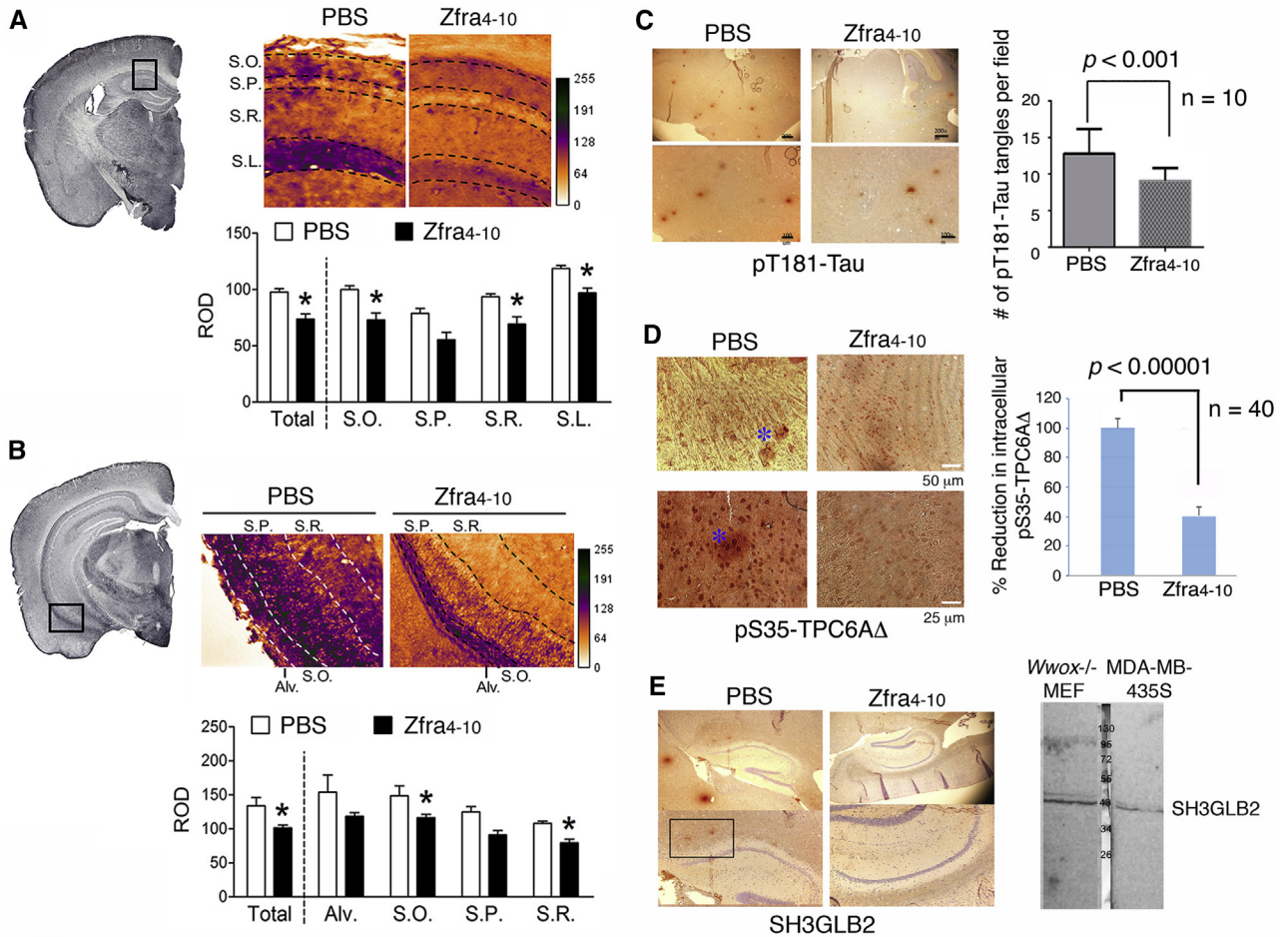
Fig. 3. Effect of Zfra on tau phosphorylation of the dorsal part hippocampi in 3×Tg mice. Representative micrographs of pS412-tau immunostaining are shown on the left panels, the boxed regions are enlarged and shown on the right, and the quantitative results are shown on the bottom. (A) Dorsal hippocampus. (B) Ventral hippocampus. *$P < .05$ versus respective PBS group, two-tailed Mann–Whitney test. (C) Zfra inhibition of pT181-tau aggregation is shown (scale bar = 200 μm for top panel and 100 μm for bottom panel). (D) Zfra suppressed intracellular pS35-TPC6AΔ expression (40 neurons counted) and extracellular pS35-TPC6AΔ plaque formation (see the blue asterisk). (E) Zfra blocked the aggregation of self-polymerizing SH3GLB2 (∼70% suppression). The quality of homemade antibody is shown. Magnification: top panel 20× and bottom panel 100×. Abbreviations: Alv., alveus; S.L., stratum lacunosum; S.O., stratum oriens; S.P., stratum pyramidale; S.R., stratum radiatum; Zfra, zinc finger-like protein that regulates apoptosis.

(control: 18.5 ± 6.5, $n = 3$; Zfra: 22.3 ± 6.7, $n = 5$; two-tailed Student t-test: $t = 0.4$, $P > .5$), indicating that no neurogenesis occurs.

3.4. Zfra suppresses melanoma growth and melanoma-induced neurodegeneration in the brain, which correlates with suppression of Ser14 phosphorylation of WWOX

Growing tumors, for example, melanoma and glioblastoma, are shown to induce neurodegeneration in vivo [37–39]. Nude mice received Zfra4–10 via tail veins for 3 consecutive weeks and then allowed to rest for a week, followed by inoculating melanoma B16F10 cells on both flanks. Melanoma grew as a solid tumor in the skin and induced apoptosis of pyramidal neurons, possessing condensed cell body and nuclei, in the hippocampi of control mice ($97 \pm 2\%$ apoptotic nuclei), whereas Zfra-

pretreated mice had no neuronal death ($0 \pm 1\%$ apoptotic nuclei) (Fig. 4A; top panel). The blocking of neuronal death correlates with Zfra-mediated significant suppression of Ser14 phosphorylation of WWOX (pS14-WWOX; $87 \pm 5\%$ suppression, $n = 3$), compared to controls ($2 \pm 3\%$ suppression, $n = 3$). Furthermore, no suppression of Tyr33 phosphorylation in WWOX by Zfra was observed ($2 \pm 6\%$ suppression, $n = 3$; data not shown). B16F10 cells did not appear to migrate to the brain (Fig. 4A).

In the cortex, B16F10 induced the formation of TPC6AΔ-containing plaques in the control mice, but not in the Zfra-treated mice (Fig. 4A; bottom panel). The tissue section was stained with a specific antibody against TRAPPC6AΔ [17–19]. TRAPPC6AΔ binds TIAF1, and the complex forms plaques in the extracellular matrix of brain cortex [17–20,33].
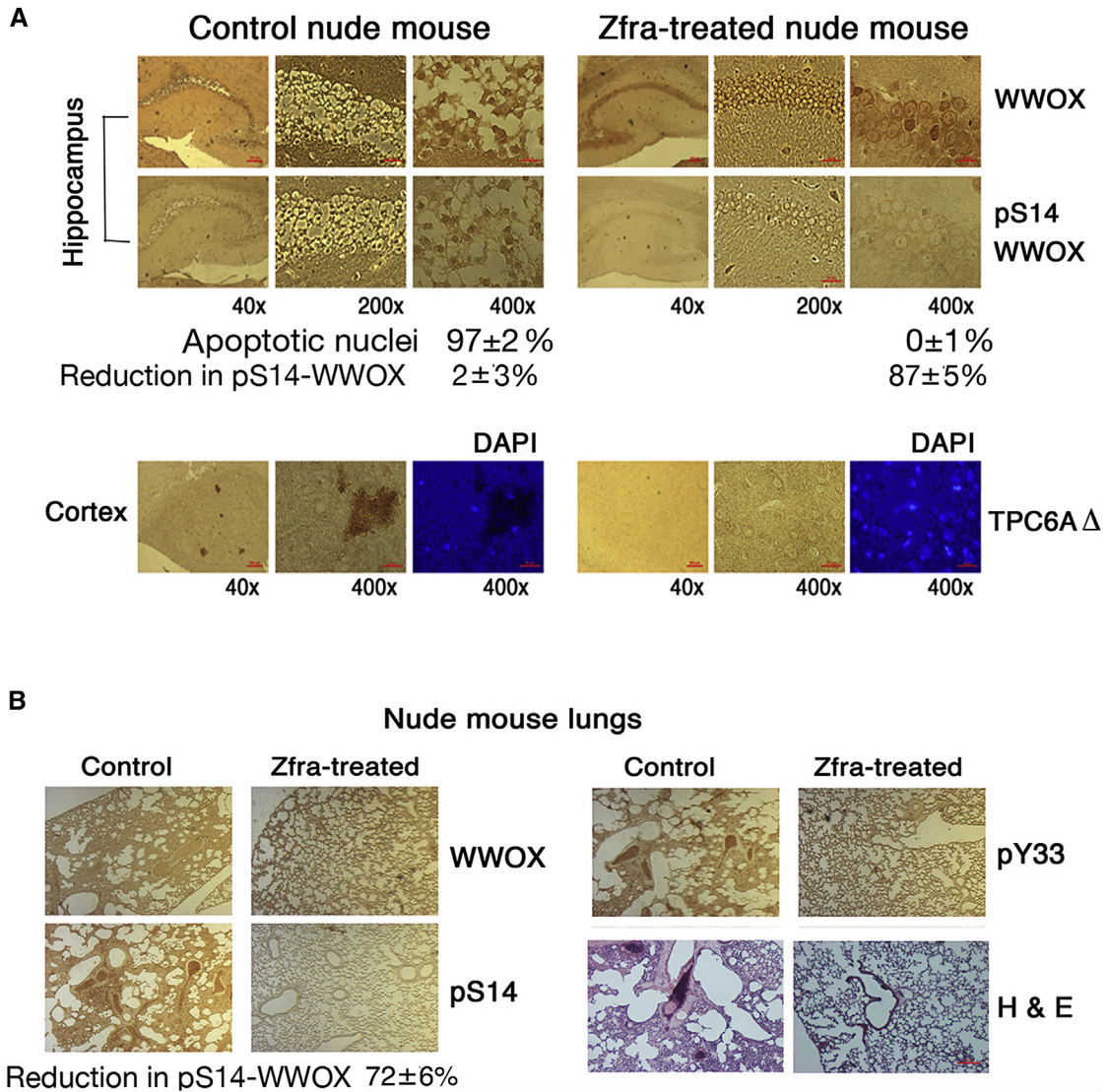
Fig. 4. Zfra suppresses melanoma B16F10-mediated neurodegeneration in the hippocampus. Nude mice were preinjected with 100 μL of sterile Milli-Q water or Zfra4–10 (1 mM in sterile water) in 3 consecutive weeks. After treatment for a week, these mice were inoculated with melanoma B16F10 cells on both flanks (2 × 10^5 cells in 100-μL PBS). Mice were sacrificed when the tumor sizes grew up to 2000–3000 mm^3 in about a month. (A) Zfra blocked neurodegeneration in the hippocampus (top panel) and prevented the formation of TPC6AΔ plaques in the cortex (bottom panel), which negatively correlates with pS14-WWOX expression. Note the presence of condensed apoptotic nuclei in the hippocampal neurons in the control mice. (B) Metastasis of B16F10 cells to the lung was blocked in Zfra-treated mice. Compared to controls, Zfra suppressed p-S14WWOX expression in the lung by ~72% suppression (three sections). The WWOX protein levels were not suppressed. Abbreviation: Zfra, zinc finger-like protein that regulates apoptosis.

In agreement with our previous report [24], Zfra4–10 blocked B16F10 metastasis to the lung (Fig. 4B). Zfra-treated mice exhibited inhibition of Ser14 phosphorylation of WWOX in the lung by greater than $72 \pm 6\%$ ($n = 3$). Zfra4–10 did not suppress the phosphorylation in Tyr33 in WWOX ($5 \pm 3\%$, $n = 3$). Tyr33 phosphorylation is a marker for WWOX activation for nuclear accumulation and inducing apoptosis when overexpressed [9,10,21,22,26]. In control mice, pSer14-WWOX was expressed in the lung, and B16F10 cells infiltrated in this organ successfully (data not shown). Together, there is a positive correlation between the expression of pS14-WWOX and the occurrence of

cancer growth and neurodegeneration in the hippocampus and plaque formation in the cortex. Comparable results were observed using the full-length Zfra1–31 in similar experiments (data not shown).

3.5. Wwox heterozygous mice exhibit enhanced memory decline

WWOX plays a critical role in the development of neural diseases and degeneration [9–19]. In light of the aforementioned observations (Fig. 4), we determined that *Wwox* heterozygous mice exhibited an age-related faster

decline in both short- and long-term memories than those in 3×Tg mice, as determined by novel object recognition tests (Supplementary Fig. 1).

3.6. Zfra blocks aggregation of Aβ and serine-containing TPC6AΔ segments in vitro

We investigated whether Zfra blocks Aβ and TPC6AΔ aggregation in vitro. By mixing Zfra and Aβ together (100 μM each peptide) and incubated in the room temperature for 24 hours or less, we showed that full-length Zfra or red-fluorescent TMR-Zfra blocked the aggregation of Aβ42 in vitro (Fig. 5A). As a negative control, Aβ40 was used (Fig. 5A).

To determine how TPC6AΔ becomes aggregated in vivo (Fig. 4B), we selected serine-containing TPC6AΔ segments and made peptides, including TPC6AΔ24-38, pS35-TPC6AΔ24-38, and TPC6AΔ84-100. The reason for choosing serine-containing segments is that these regions tend to undergo aggregation. For example, when the aforementioned peptides were suspended in PBS, they became aggregated (Fig. 5B). Little or no aggregations were shown when these peptides were suspended in Milli-Q water (Fig. 5B). By mixing these TPC6AΔ peptides with Zfra4–10, Zfra4–10 effectively blocked the aggregation of TPC6AΔ peptides (Fig. 5B). These observations suggest that Zfra4–10 blocks TPC6AΔ aggregation in vivo via interactions with the serine-containing TPC6AΔ segments.

Under similar conditions, we synthesized serine-containing WWOX7-21, WWOX286-299, and ANK RD40266-281 peptides, along with specific phosphorylation at Ser14, Tyr287, and Ser271, respectively. Without phosphorylation, these peptides polymerized in PBS, and Zfra4–10 effectively blocked the polymerization or aggregation (Fig. 5C). ANKRD40 is Ankyrin Repeat Domain 40, whose function is largely unknown. Phosphorylation in WWOX7-21 and ANKRD40266-281 reduced their extent of polymerization in PBS, and Zfra4–10 had apparent effects (Fig. 5C). However, pY287-WWOX286-299 became aggregated in PBS and Zfra4–10 did not effectively block the aggregation (Fig. 5C).

3.7. Zfra covalently cross-links cellular proteins and accelerates their degradation

To continue to investigate how Zfra reduces protein aggregation in vivo, we examined whether Zfra interacts with cytosolic proteins and accelerates protein degradation. Zfra peptide at high concentrations may undergo self-polymerization especially in PBS [24]. When full-length Zfra1–31 peptide (∼85% pure; >1 mM) was resuspended in PBS, it underwent self-polymerization with increasing molecular sizes from 3.5 kDa up to 78 and 80 kDa, as analyzed by reducing SDS-PAGE (see the vertical arrow at lane 10, and also lanes 1, 4, and 7; Fig. 6A). Zfra-deficient

human breast MCF7 cells were used [1]. Cell lysates were prepared and incubated with Zfra1–31, in the presence or absence of a proteasome inhibitor MG-132 and an aliquot of a cocktail of protease inhibitors. The results showed that Zfra-bound cellular proteins as it migrated higher than 3.5 kDa, and the complexes resisted dissociation by SDS and β-mercaptoethanol. We hereby designated the Zfra-bound proteins are "zfrated." The zfrated proteins were degraded with time of incubation (Fig. 6A). Notably, MG-132 did not block but enhanced the protein degradation (see the 30-kDa protein in lanes 2 and 3), suggesting that the ubiquitin/proteasome system is not involved in the degradation process (Fig. 6A). In addition, zfrated proteins from the whole cell lysates or immunoprecipitation did not contain ubiquitin, as determined by antibodies against ubiquitin, and ubiquitin with K48 or K63 acetylation (data not shown).

Similarly, Zfra-negative DU145 cells were exposed to UV light and incubated for 30 minutes at 37°C [1]. Whole cell lysates were prepared in the presence of a cocktail of protease inhibitors. Incubation of the cell lysates with Zfra rapidly increased zfration of cellular proteins (e.g., 78, 80, 200 kDa, and many minor band) in 1–20 minutes, as determined by reducing SDS-PAGE (Fig. 6B). Despite the presence of protease inhibitors, the protein complexes underwent degradation approximately by 60% in 40 minutes and near 95% in 1–2 hours at 37°C (Fig. 6C). The observations suggest the presence of unidentified proteases in degrading the zfrated proteins. Exogenous Zfra alone also underwent degradation, which is in agreement with our previous report [3]. In controls, Zfra-free lysates had significantly retarded degradation in the presence of protease inhibitors (<10% in 1–2 hours).

Murine L929 fibroblasts express low levels of Zfra. UV irradiation or TNF-α upregulates the expression of Zfra [1,2]. Aliquots of the lysates of L929 cells were incubated with Zfra1–31 peptide for 30 minutes at 37°C (in PBS). Two proteins of 80 and 22 kDa were rapidly zfrated and then degraded in 30 minutes (Fig. 6D). In addition, a 30-kDa protein became zfrated during incubation for 30 minutes (Fig. 6D). We further verified zfration using purified small recombinant proteins. Zfra caused zfration of recombinant His-Tau in PBS, as determined by reducing SDS-PAGE (Fig. 6E).

3.8. Endogenous Zfra binds tau and Aβ in the AD hippocampus

We examined the levels of Zfra in the hippocampal extracts from postmortem AD patients and normal controls. By immunofluorescence and confocal microscopy, Zfra was shown to colocalize with Aβ and PHF (paired helical filaments)-tau (Fig. 7A–D). Binding of Zfra with Aβ and PHF-tau was verified by Förster resonance energy transfer
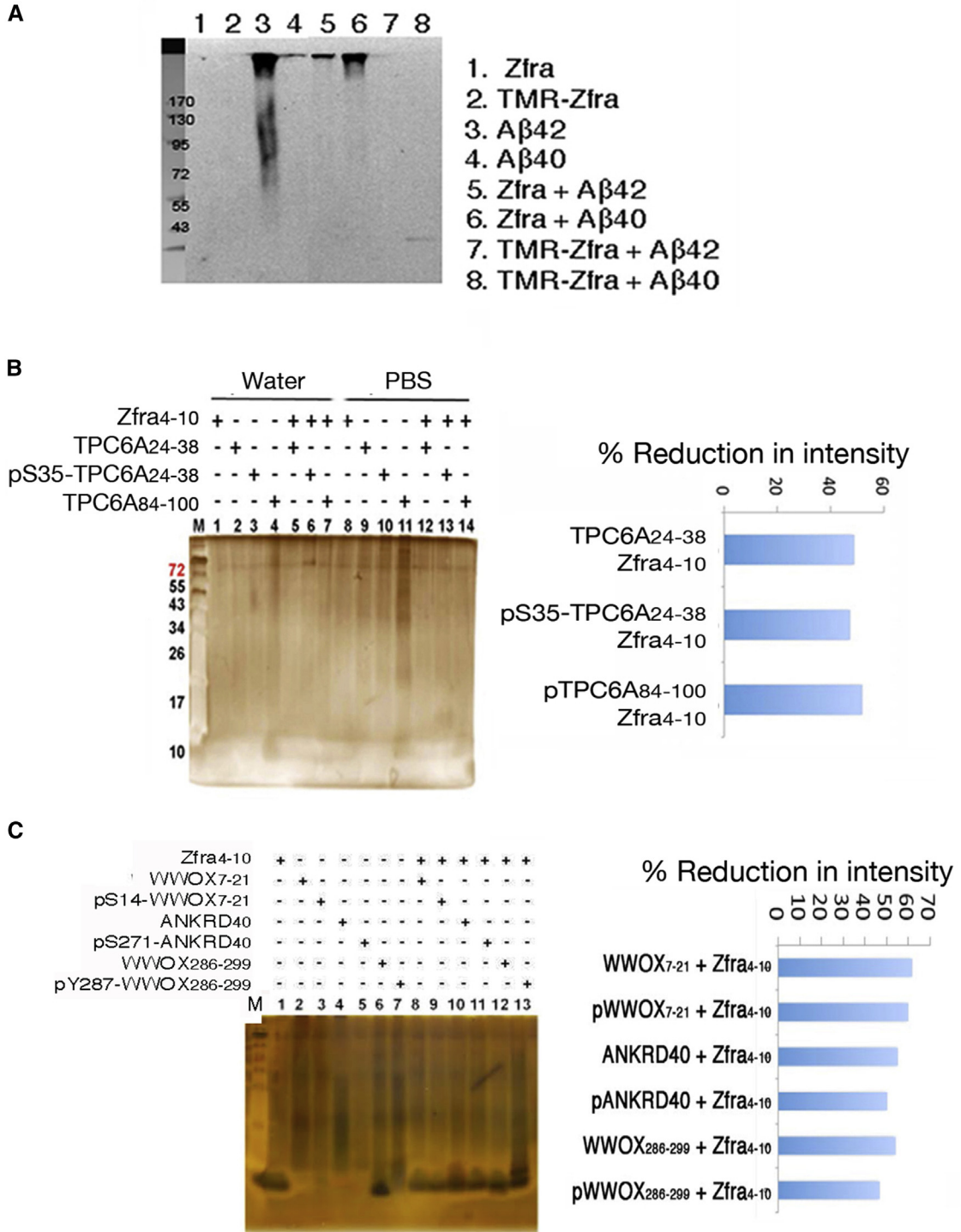
Fig. 5. Zfra suppresses polymerization or aggregation of serine-containing TPC6AΔ and other peptides in PBS. Zfra4–10 was incubated with an indicated serine-containing peptide in PBS at room temperature for 24 hours (final 200 μM each peptide). The mixtures were subjected to nonreducing sodium dodecyl sulfate polyacrylamide gel electrophoresis (SDS-PAGE). (A) Full-length Zfra or red-fluorescent TMR-Zfra blocked aggregation of Aβ42 (lanes 3, 5, and 7). In controls, Aβ40 did not undergo aggregation. The membrane was stained with antibody against Aβ. (B) Zfra4–10 and one of the TPC6AΔ peptides were resuspended in Milli-Q water or PBS and incubated for 24 hours at room temperature. Zfra4–10 suppressed the polymerization of serine-containing peptides. % Reduction in intensity = $[1 - (Z.P)/(Z + P)] \times 100\%$, where Z = Zfra4–10, P = an indicated peptide, and Z.P = peptide mixture. (C) Under similar conditions, serine-containing peptides derived from WWOX and ANKRD40 were synthesized, possessing with or without phosphorylation at a specific serine or tyrosine residue. Zfra4–10 suppressed polymerization of these peptides in PBS. Abbreviation: Zfra, zinc finger-like protein that regulates apoptosis.
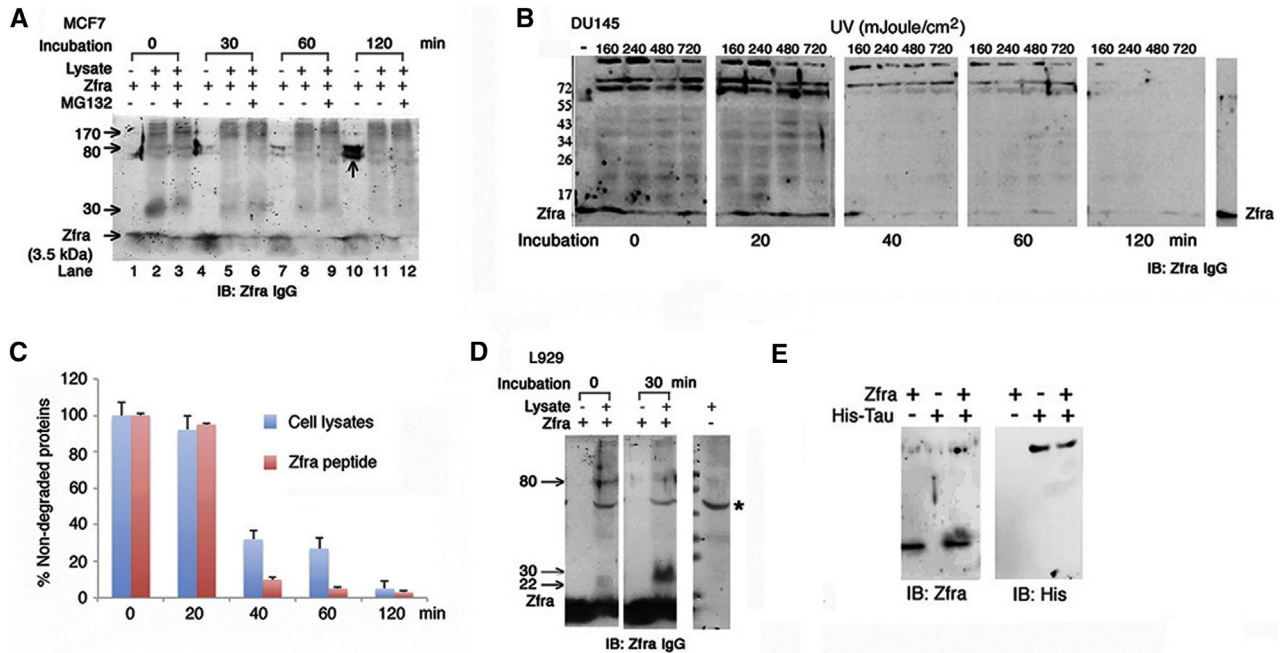
Fig. 6. Zfra covalently binds and accelerates protein degradation. (A) On dissolving in PBS for 30–120 minutes at 37°C, Zfra peptide (3.5 kDa) underwent self-polymerization and formed large-size complexes (78 and 80 kDa), as determined by reducing SDS-PAGE and Western blotting (see the vertical arrow at lane 10, and lanes 1, 4, and 7). Aliquots of Zfra-deficient breast MCF7 cell lysates (100 μg) were incubated with Zfra (100 μM) for various durations in the presence or absence of proteasome inhibitor MG-132 (50 μM). Zfra formed complexes with cytosolic proteins (or zfrated; see arrows), and disappeared with time even in the presence of MG-132. (B and C) Zfra-negative prostate DU145 cells were exposed to UV (160–720 mJ/cm^2), and aliquots of whole cell lysates (100 μg) were incubated with Zfra peptide (100 μM) for various durations (in PBS) at 37°C, in the presence of a cocktail of protease inhibitors (1:10 dilution). Zfrated proteins (70, 72, 200 kDa and minor band ladders) and exogenous Zfra peptide were degraded with time (>99% in 120 minutes; reducing SDS-PAGE). Synthetic Zfra was in PBS at the first lane at the left, and in Milli-Q water at the last lane at the right. Zfra-free control lysates had only less than 10% degradation of total proteins after incubation for 120 minutes, in the presence of protease inhibitors (data not shown). (D) L929 cell lysates (100 μg) were incubated with Zfra peptide (100 μM) for 30 minutes at 37°C (in PBS). A 30-kDa protein was zfrated in 30 minutes, and 22- and 80-kDa protein was zfrated rapidly and then degraded in 30 minutes (reducing SDS-PAGE). *A nonspecific immunoreactive or a zfrated protein in L929 cells. (E) Zfra peptide (100 μM) bound recombinant His-Tau (2 μg protein) in PBS for 24 hours at room temperature, and the resulting complex resisted dissociation by reducing SDS-PAGE. Abbreviation: Zfra, zinc finger-like protein that regulates apoptosis.

(FRET) analysis [18,20,26,39]. In most cases, Zfra bound strongly with Aβ and PHF-tau, or no binding at all (see FRETc) (Fig. 7E). Confocal microscopy analysis revealed the colocalization of Zfra with Aβ (Fig. 7C). Similarly, by using postmortem human soluble hippocampal extracts, endogenous Zfra was shown to complex, in part, with Aβ, as determined by nonreducing SDS-PAGE (data not shown). By filter retardation assay using insoluble hippocampal extracts [10,17], aggregation of Zfra and pSer8-Zfra occurred greatly by 45% and 85% increases, respectively, in the older AD patients (81 ± 9.7 years old; n = 70), as compared to younger nondemented controls (60 ± 13.3 years old; n = 46) (Fig. 7F). In the AD hippocampi, Aβ levels were raised by 170%.

3.9. Zfra blocks TNF-mediated activation of NF-κB promoter

NF-κB plays a crucial role in the pathogenesis of AD [40]. We examined whether Zfra blocks NF-κB promoter

activation using a fluorescent reporter assay [41]. COS7 fibroblasts were transfected with a GFP-tagged NF-κB promoter reporter construct and/or an ECFP-Zfra construct. In controls, cells were transfected with a negative or a positive GFP control vector, or an empty ECFP vector. These cells were exposed to TNF-α for 24 hours. Zfra blocked TNF-α-mediated activation of NF-κB promoter in cells expressing ECFP-Zfra and the promoter construct (Fig. 7G). In controls, TNF-α–activated NF-κB promoter in cells transfected the promoter construct, in the presence or absence of ECFP (Fig. 7G).

3.10. Zfra induces Z cells to relocate out of the spleen and does not appear to migrate to the brain

When immune-competent or deficient mice receive Zfra via tail vein injections, circulating Zfra is mainly deposited in the spleen and fluoresced strongly due to aggregation [17]. Zfra activates Z cell to induce memory response against the growth of many types of cancer
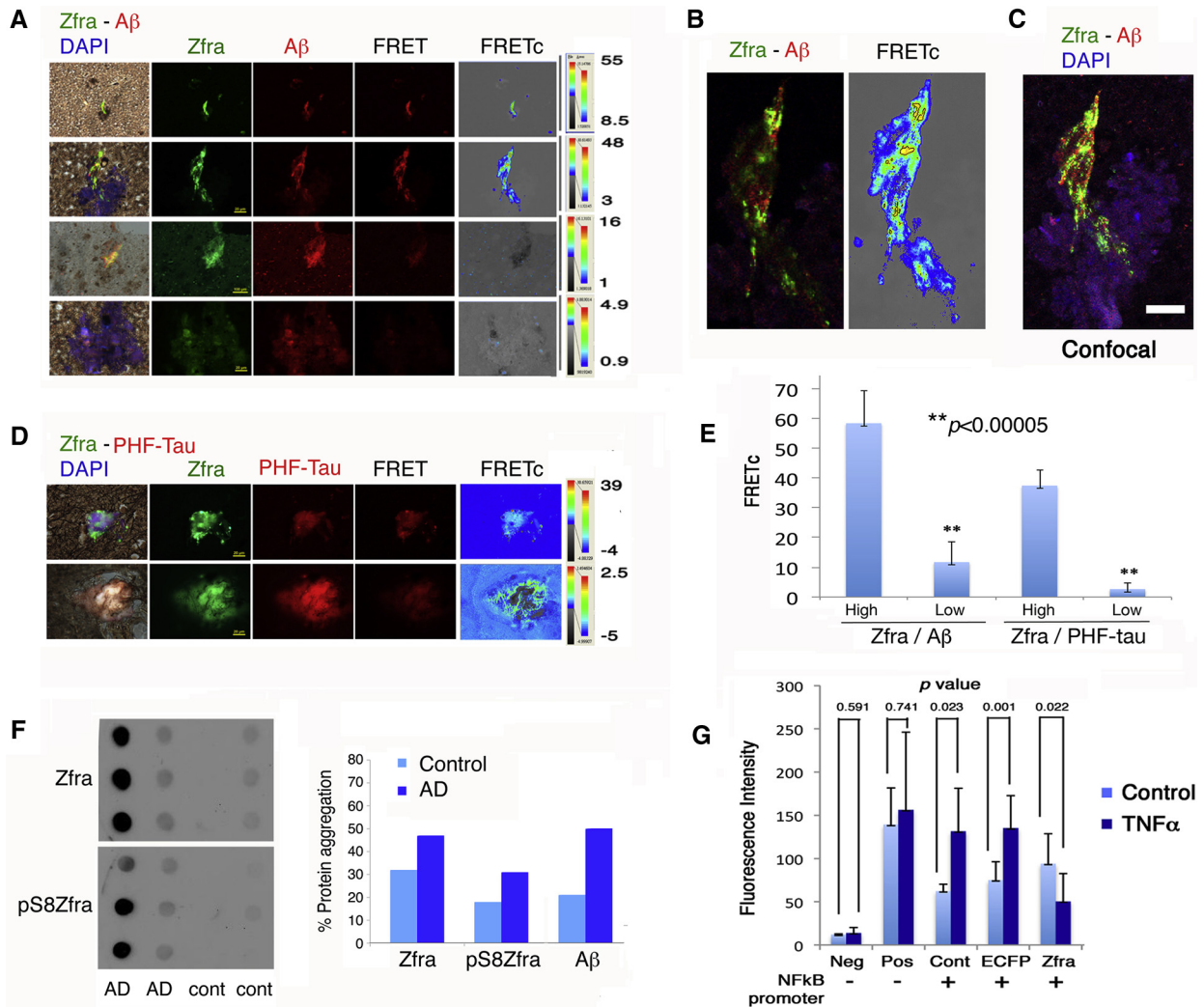
Fig. 7. Zfra is upregulated in the AD hippocampi and interacts with tau and Aβ and blocks NF-κB promoter activation. (A and B) By antibody FRET microscopy, Zfra bound Aβ with a high affinity (FRETc greater than 45) in the hippocampal sections of postmortem AD patients (see yellow punctates in B). However, Zfra may colocalize with Aβ but without binding (FRETc less than 5). (C) Confocal microscopy analysis revealed the colocalization of Zfra with Aβ. (D) Zfra binds PHF-tau with a similar pattern. (E) A bar graph of Zfra binding with Aβ or PHF-tau is shown ($n = 20$). (F) By filter retardation assay using insoluble human hippocampal extracts, aggregation of Zfra and pSer8-Zfra was increased by 45 and 85%, respectively, in the older AD patients (81 ± 9.7 years old; $n = 70$), compared to younger nondemented controls (60 ± 13.3 years old; $n = 46$). Aβ was increased by 170% in the AD patients. (G) Zfra significantly blocked TNF-α (50 ng/mL)-mediated activation of NF-κB promoter in COS7 cells. Abbreviations: AD, Alzheimer's disease; Neg, negative control; PHF, paired helical filament; Pos, positive control; Zfra, zinc finger-like protein that regulates apoptosis.

cells [17]. Residential Z cells are localized in the peripheral areas of germinal centers in the 3×Tg mice, and that Zfra drove the cells out of the spleen (Fig. 8A). Similar results were observed in other immune-competent mice (e.g., BALB/c and B6 mice). Z cells did not appear to migrate to the brain, as the signals were barely detectable (Fig. 8B). In the T cell–deficient nude mice, the residential Z cell population exhibited as clusters (Fig. 8C). These mice do not have germinal centers. In response to Zfra, Z cells moved out of the spleen in the nude mice and relocated, in part, in the cancer lesion sites (Fig. 8D). Z cells localized in the lymphatic ducts penetrating in the skin B16F10 tumors (Fig. 8D).

In control mice, less Z cells relocated to the tumor lesions.

4. Discussion

In summary, we demonstrated here for the first time that Zfra effectively restores the memory capabilities of aging Alzheimer's disease 3×Tg mice. The underlying mechanism is associated, in part, with Zfra inhibition of the aggregation of TPC6AΔ, SH3GLB2, tau, and Aβ in the mouse brains. In vitro assays showed Zfra suppression of TNF-mediated NF-κB activation, suggesting an additional mechanism of Zfra inhibition of inflammatory NF-κB activation in AD
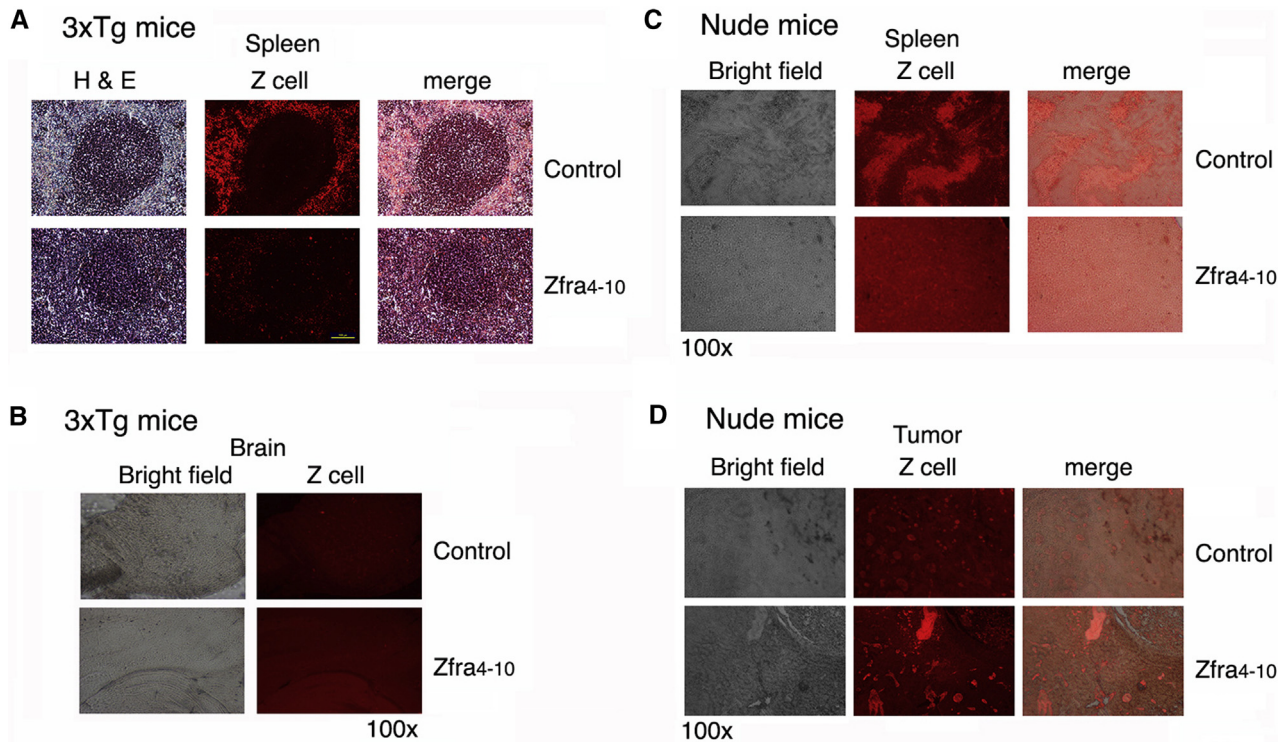
Fig. 8. Zfra induces spleen Z cells to relocate out of the spleen, but the cells do not appear to migrate to the brain. (A) Spleen sections from Zfra-treated and control 3×Tg mice were stained with TMR-Zfra, followed by determining the presence of Z cells by fluorescence microscopy. Z-cell migration out of the spleen is shown in the Zfra-treated 3×Tg mice. Scale bar is 100 μm in length (100× magnification). (B) Similar experiments were carried out using brain tissue sections of 3×Tg mice. Brain sections were examined. (C and D) Similarly, spleens were harvested from Zfra-treated and control nude mice, which were inoculated with melanoma B16F10. Zfra induced Z-cell relocation out of the spleen, and the cells were found in the skin cancer lesions. Abbreviations: TMR-Zfra, tetramethylrhodamine-labeled Zfra; Zfra, zinc finger-like protein that regulates apoptosis.

brains in vivo. SH3GLB2 is abundant in the hippocampus (data not shown). How SH3GLB2 polymerization contributes to neurodegeneration is being determined in our laboratories.

In the melanoma mouse model, we showed that Zfra blocks neuronal death in the hippocampus and plaque formation in the cortex. No neurogenesis occurs in hippocampal subgranular and subventricular zones. Additional evidence showed that Zfra inhibits the aggregation of Aβ42, TPC6AΔ, and many serine-containing peptides under cell-free conditions. Preliminary data by mass analysis showed that covalent cross-linking between serine residues occurs, especially in the presence of phosphates in the solution (data not shown). Zfra binds cytosolic proteins to accelerate their degradation in vitro, which may reduce the levels of aggregated TPC6AΔ, tau, and Aβ in vivo. We determined that the protein ubiquitination/proteosomal system does not participate in the Zfra-regulated degradation processes.

Participation of Z cells in reducing protein aggregation is very likely. Circulating Zfra is mainly deposited in the spleen [24]. We do not exclude the possibility that a small amount of Zfra goes through the blood–brain barrier and targets tau or Aβ for accelerating degradation. A portion

of WWOX is present on the cell membrane via interacting with Hyal-2 and Ezrin [25,27,41–43]. Zfra activates Z cells in the spleen probably via the Hyal-2/WWOX/Smad4 pathway [25,27,41,42]. Approximately in 3 weeks or less, these activated Z cells leave the spleen and enter the lymphatic ducts. Whether these cells stay in the lymphatic nodes or other organs is unknown. In cancer experiments, Z cells infiltrate in the cancer lesions via lymphatic ductules. However, Z cells do not appear to relocate to the brain. Conceivably, Z cells secreted cytokines or proteases capable of degrading protein aggregates in the brain. In addition, we have been carrying out transfer of activated Z cells to aging 3×Tg mice to validate their function in blocking neurodegeneration.

To gain a better insight regarding how Zfra works in AD brains, we examined hippocampal extractions from post-mortem normal individuals and AD patients [17,20]. We found that upregulation of Zfra, pS8-Zfra, and Aβ in the AD hippocampi occurs and these proteins are found in the insoluble fractions. The observations suggest that during AD progression, the levels of Zfra could be too low to tackle protein aggregation, or Zfra is inactivated by coaggregation

with tau or Aβ. Indeed, when 3×Tg mice are at age 12 months, injected Zfra fails to restore memory deficit, suggesting that when there are too much accumulation of tau and Aβ, Zfra may not be able to increase protein degradation effectively.

We found that the AD-related pathologies are not uniformly distributed in the hippocampal subregions. The pTau signals are mainly localized in the stratum oriens, stratum radiatum, and stratum lacunosum regions, which are in agreement with findings of AD pathology that neurofibrillary tau burden in the hippocampus is frequently restricted to the stratum radiatum and stratum lacunosum and good correlations with clinical dementia ratings [34,44]. Hyperphosphorylated tau in the stratum radiatum and stratum lacunosum regions is associated with the Consortium to Establish a Registry for Alzheimer's Disease diagnosis and age of onset [45]. Moreover, postmortem examination of AD brains reveals that the volumes of stratum radiatum and stratum lacunosum are significantly reduced in AD brains, whereas the volumes of other hippocampal subregions, such as alveus and stratum pyramidale, are similar between AD and age-matched, cognitively intact controls [46]. Synaptic losses in the stratum radiatum and stratum lacunosum occur much earlier than that in the stratum pyramidale [34,35]. Stratum oriens and stratum radiatum are involved in the perforant pathway of entorhinal cortex-CA region [35], suggesting that the perforant pathway abnormalities are an anatomical substrate of memory deficit in the prodromal phase of AD [47].

Diseased organs frequently exhibit increased expression of pS14-WWOX (article in preparation). pS14-WWOX-expressing organs tend to be susceptible for cancer cell docking and homing. We used the melanoma-induced neurodegeneration model in mice and determined the therapeutic efficacy of Zfra in blocking neuronal death. Zfra inhibits WWOX phosphorylation at Ser14 in the brain and lung, and this positively correlates with suppression of cancer-induced neurodegeneration in the hippocampus and plaque formation in the cortex, and inhibition of cancer cell metastasis to the lung. Without Zfra treatment, control mice had melanoma metastasis to the lung and neurodegeneration in the brain, plus increased pS14-WWOX expression in these organs. Intriguingly, upregulation of Ser14 phosphorylation in WWOX drives leukemia T cell to maturation [27]. Further studies are needed to establish the Ser14 phosphorylation in WWOX in organs and correlation with disease susceptibility. In addition, by using *Wwox* heterozygous mice, we determined that decline of memory is faster than those of 3×Tg mice. The observations provide another line of evidence that WWOX is essential in supporting neuronal functions. Knockout *Wwox* mice have brain developmental defects, ataxia and seizure. They can only survive for less than

30 days [17]. They are not suitable for the intended experiments for memory decline.

As short as seven amino acids, Zfra4–10 undergoes self-polymerization and is highly potent in blocking many types of cancer metastasis and growth [24]. Zfra4–10 is effective in restoring the memory deficits in 3×Tg mice and blocks cancer-associated neurodegeneration. The conserved phosphorylation site Ser8 plays a crucial role in conferring polymerization of Zfra4–10, as determined by LC/MS/MS (article in preparation). When Zfra peptide is mixed with a serine-containing peptide, polymerization of both peptides is nullified.

We have mapped the expression of WWOX from embryonic development to newborns in mice [48]. In the adult brain, WWOX is expressed mainly in the epithelial cells of the choroids plexus and ependymal cells. The *N*-terminal WW domain of WWOX has three antiparallel sheets. Zfra binds to the first WW domain [1–4]. Aggregation of this first WW domain region may occur under pathological conditions. A portion of endogenous WWOX is anchored on the cell membrane [41,42]. Presumably, Zfra binds aggregated WWOX and the complex is subjected to degradation in the AD brain.

Supplementary data

Supplementary data related to this article can be found at http://dx.doi.org/10.1016/j.trci.2017.02.001.

RESEARCH IN CONTEXT

1. Systematic review: We have shown the strong efficacy of synthetic Zfra peptides in restoring memory deficits in Alzheimer's $3\times$Tg mice. Zfra is a naturally occurring small peptide and is known to prevent and cure many types of cancers. Zfra is now shown to exhibit a strong potential in the therapy for AD.

2. Interpretation: Zfra acts by blocking the aggregation of TPC6AΔ, SH3GLB2, tau, and formation of amyloid plaques in $3\times$Tg mice and restores their memory deficits. Zfra also blocks neurodegeneration caused by melanoma and glioblastoma. Mechanistically, Zfra blocks the aggregation of Aβ42 peptide and many serine-containing peptides, accelerates protein degradation, and inhibits TNF-mediated activation of NF-κB promoter activation from many in vitro experiments. These in vitro observations suggest how Zfra peptide works in vivo.

3. Future directions: While Zfra is currently at a stage of Investigational New Drug for cancer treatment, it is necessary to initiate intensive study for Zfra in curing AD in large-size animals before clinical trial in AD patients. Furthermore, mechanistic insights regarding how Zfra works in vivo need to be further elucidated.

References

[1] Hsu LJ, Schultz L, Mattison J, Lin YS, Chang NS. Cloning and characterization of a small-size peptide Zfra that regulates the cytotoxic function of tumor necrosis factor by interacting with JNK1. Biochem Biophys Res Commun 2005;327:415–23.

[2] Hong Q, Hsu LJ, Schultz L, Pratt N, Mattison J, Chang NS. Zfra affects TNF-mediated cell death by interacting with death domain protein TRADD and negatively regulates the activation of NF-kappaB, JNK1, p53 and WOX1 during stress response. BMC Mol Biol 2007;8:50.

[3] Hsu LJ, Hong Q, Schultz L, Kuo E, Lin SR, Lee MH, et al. Zfra is an inhibitor of Bcl-2 expression and cytochrome c release from the mitochondria. Cell Signal 2008;20:1303–12.

[4] Dudekula S, Lee MH, Hsu LJ, Chen SJ, Chang NS. Zfra is a small wizard in the mitochondrial apoptosis. Aging (Albany NY) 2010;2:1023–9.

[5] Chang NS, Hsu LJ, Lin YS, Lai FJ, Sheu HM. WW domain-containing oxidoreductase: a candidate tumor suppressor. Trends Mol Med 2007; 13:12–22.

[6] Abu-Remaileh M, Joy-Dodson E, Schueler-Furman O, Aqeilan RI. Pleiotropic functions of tumor suppressor WWOX in normal and cancer cells. J Biol Chem 2015;290:30728–35.

[7] Chang JY, He RY, Lin HP, Hsu LJ, Lai FJ, Hong Q, et al. Signaling from membrane receptors to tumor suppressor WW domain-containing oxidoreductase. Exp Biol Med (Maywood) 2010;235:796–804.

[8] Chang NS. Introduction to a thematic issue for WWOX. Exp Biol Med (Maywood) 2015;240:281–4.

[9] Chang HT, Liu CC, Chen ST, Yap YV, Chang NS, Sze CI. WW domain-containing oxidoreductase in neuronal injury and neurological diseases. Oncotarget 2014;5:11792–9.

[10] Sze CI, Su M, Pugazhenthi S, Jambal P, Hsu LJ, Heath J, et al. Down-regulation of WW domain-containing oxidoreductase induces Tau phosphorylation in vitro. A potential role in Alzheimer's disease. J Biol Chem 2004;279:30498–506.

[11] Wang HY, Juo LI, Lin YT, Hsiao M, Lin JT, Tsai CH, et al. WW domain-containing oxidoreductase promotes neuronal differentiation via negative regulation of glycogen synthase kinase 3beta. Cell Death Differ 2012;19:1049–59.

[12] Chang NS. In Memoriam: Shur-Tzu (Su) Chen, a pioneer in tumor suppressor WWOX for neuroscience. J Biomed Sci 2015;22:39.

[13] Suzuki H, Katayama K, Takenaka M, Amakasu K, Saito K, Suzuki K. A spontaneous mutation of the Wwox gene and audiogenic seizures in rats with lethal dwarfism and epilepsy. Genes Brain Behav 2009; 8:650–60.

[14] Mallaret M, Synofzik M, Lee J, Sagum CA, Mahajnah M, Sharkia R, et al. The tumour suppressor gene WWOX is mutated in autosomal recessive cerebellar ataxia with epilepsy and mental retardation. Brain 2014;137:411–9.

[15] Tabarki B, AlHashem A, AlShahwan S, Alkuraya FS, Gedela S, Zuccoli G. Severe CNS involvement in WWOX mutations: description of five new cases. Am J Med Genet A 2015;167A:3209–13.

[16] Elsaadany L, El-Said M, Ali R, Kamel H, Ben-Omran T. W44X mutation in the WWOX gene causes intractable seizures and developmental delay: a case report. BMC Med Genet 2016;17:53.

[17] Chang JY, Lee MH, Lin SR, Yang LY, Sun HS, Sze CI, et al. Trafficking protein particle complex 6A delta (TRAPPC6ADelta) is an extracellular plaque-forming protein in the brain. Oncotarget 2015; 6:3578–89.

[18] Chang JY, Chang NS. WWOX dysfunction induces sequential aggregation of TRAPPC6AΔ, TIAF1, tau and amyloid β, and causes apoptosis. Cell Death Discov 2015;1:15003.

[19] Sze CI, Kuo YM, Hsu LJ, Fu TF, Chiang MF, Chang JY, et al. A cascade of protein aggregation bombards mitochondria for neurodegeneration and apoptosis under WWOX deficiency. Cell Death Dis 2015;6:e1881.

[20] Chang JY, Chiang MF, Lin SR, Lee MH, He H, Chou PY, et al. TIAF1 self-aggregation in peritumor capsule formation, spontaneous activation of SMAD-responsive promoter in p53-deficient environment, and cell death. Cell Death Dis 2012;3:e302.

[21] Chang NS, Pratt N, Heath J, Schultz L, Sleve D, Carey GB, et al. Hyaluronidase induction of a WW domain-containing oxidoreductase that enhances tumor necrosis factor cytotoxicity. J Biol Chem 2001; 276:3361–70.

[22] Chang NS. A potential role of p53 and WOX1 in mitochondrial apoptosis (review). Int J Mol Med 2002;9:19–24.

[23] Choo A, O'Keefe LV, Lee CS, Gregory SL, Shaukat Z, Colella A, et al. Tumor suppressor WWOX moderates the mitochondrial respiratory complex. Genes Chromosomes Cancer 2015;54:745–61.

[24] Lee MH, Su WP, Wang WJ, Lin SR, Lu CY, Chen YA, et al. Zfra activates memory Hyal-2+ CD3- CD19- spleen cells to block cancer growth, stemness, and metastasis in vivo. Oncotarget 2015;6:3737–51.

[25] Su WP, Wang WJ, Sze CI, Chang NS. Zfra induction of memory anticancer response via a novel immune cell. Oncoimmunology 2016;5:9.

[26] Chang NS, Doherty J, Ensign A. JNK1 physically interacts with WW domain-containing oxidoreductase (WOX1) and inhibits WOX1-mediated apoptosis. J Biol Chem 2003;278:9195–202.

[27] Huang SS, Su WP, Lin HP, Kuo HL, Wei HL, Chang NS. Role of WW domain-containing oxidoreductase WWOX in driving T cell acute lymphoblastic leukemia maturation. J Biol Chem 2016;291:17319–31.

[28] Oddo S, Caccamo A, Shepherd JD, Murphy MP, Golde TE, Kayed R, et al. Triple-transgenic model of Alzheimer's disease with plaques and tangles: intracellular Abeta and synaptic dysfunction. Neuron 2003; 39:409–21.

[29] Lin TW, Chen SJ, Huang TY, Chang CY, Chuang JI, Wu FS, et al. Different types of exercise induce differential effects on neuronal adaptations and memory performance. Neurobiol Learn Mem 2012; 97:140–7.

M.-H. Lee et al. / Alzheimer's & Dementia: Translational Research & Clinical Interventions 3 (2017) 189-204

[30] Shih YH, Tsai KJ, Lee CW, Shiesh SC, Chen WT, Pai MC, et al. Apolipoprotein C-III is an amyloid-beta-binding protein and an early marker for Alzheimer's disease. J Alzheimers Dis 2014; 41:855–65.

[31] Yang TT, Lo CP, Tsai PS, Wu SY, Wang TF, Chen YW, et al. Aging and exercise affect hippocampal neurogenesis via different mechanisms. PLoS One 2015;10:e0132152.

[32] Chu YY, Ko CY, Wang WJ, Wang SM, Gean PW, Kuo YM, et al. Astrocytic CCAAT/enhancer binding protein delta regulates neuronal viability and spatial learning ability via miR-135a. Mol Neurobiol 2016;53:4173–88.

[33] Lee MH, Lin SR, Chang JY, Schultz L, Heath J, Hsu LJ, et al. TGF-beta induces TIAF1 self-aggregation via type II receptor-independent signaling that leads to generation of amyloid beta plaques in Alzheimer's disease. Cell Death Dis 2010;1:e110.

[34] Braak E, Braak H. Alzheimer's disease: transiently developing dendritic changes in pyramidal cells of sector CA1 of the Ammon's horn. Acta Neuropathol 1997;93:323–5.

[35] Thal DR, Holzer M, Rub U, Waldmann G, Gunzel S, Zedlick D, et al. Alzheimer-related tau-pathology in the perforant path target zone and in the hippocampal stratum oriens and radiatum correlates with onset and degree of dementia. Exp Neurol 2000;163:98–110.

[36] Pierrat B, Simonen M, Cueto M, Mestan J, Ferrigno P, Heim J. SH3GLB, a new endophilin-related protein family featuring an SH3 domain. Genomics 2001;71:222–34.

[37] Lee SG, Kim K, Kegelman TP, Dash R, Das SK, Choi JK, et al. Oncogene AEG-1 promotes glioma-induced neurodegeneration by increasing glutamate excitotoxicity. Cancer Res 2011;71:6514–23.

[38] Valpione S, Zoccarato M, Parrozzani R, Pigozzo J, Giometto B, Laveder F, et al. Paraneoplastic cerebellar degeneration with anti-Yo antibodies associated with metastatic uveal melanoma. J Neurol Sci 2013;335:210–2.

[39] Emdad L, Sarkar D, Su ZZ, Lee SG, Kang DC, Bruce JN, et al. Astrocyte elevated gene-1: recent insights into a novel gene involved in tumor progression, metastasis and neurodegeneration. Pharmacol Ther 2007;114:155–70.

[40] Shi ZM, Han YW, Han XH, Zhang K, Chang YN, Hu ZM, et al. Upstream regulators and downstream effectors of NF-κB in Alzheimer's disease. J Neurol Sci 2016;366:127–34.

[41] Hsu LJ, Schultz L, Hong Q, Van Moer K, Heath J, Li MY, et al. Transforming growth factor beta1 signaling via interaction with cell surface Hyal-2 and recruitment of WWOX/WOX1. J Biol Chem 2009; 284:16049–59.

[42] Hsu LJ, Chiang MF, Sze CI, Su WP, Yap YV, Lee IT, et al. HYAL-2-WWOX-SMAD4 signaling in cell death and anticancer response. Front Cell Dev Biol 2016;4:141.

[43] Jin C, Ge L, Ding X, Chen Y, Zhu H, Ward T, et al. PKA-mediated protein phosphorylation regulates ezrin-WWOX interaction. Biochem Biophys Res Commun 2006;341:784–91.

[44] Braak H, Braak E. Neuropathological stageing of Alzheimer-related changes. Acta Neuropathol 1991;82:239–59.

[45] Seifan A, Marder KS, Mez J, Noble JM, Cortes EP, Vonsattel JP, et al. Hippocampal laminar distribution of tau relates to Alzheimer's disease and age of onset. J Alzheimers Dis 2015;43:315–24.

[46] Boutet C, Chupin M, Lehericy S, Marrakchi-Kacem L, Epelbaum S, Poupon C, et al. Detection of volume loss in hippocampal layers in Alzheimer's disease using 7 T MRI: a feasibility study. Neuroimage Clin 2014;5:341–8.

[47] Hyman BT, Van Hoesen GW, Kromer LJ, Damasio AR. Perforant pathway changes and the memory impairment of Alzheimer's disease. Ann Neurol 1986;20:472–81.

[48] Chen ST, Chuang JI, Wang JP, Tsai MS, Li H, Chang NS. Expression of WW domain-containing oxidoreductase WOX1 in the developing murine nervous system. Neuroscience 2004;124:831–9.